RSC Advances

PAPER

View Article Online
View Journal | View Issue

Cite this: *RSC Adv.*, 2020, **10**, 13936

Facile one-pot synthesis of silver nanoparticles encapsulated in natural polymeric urushiol for marine antifouling

Lu Zheng, †[ac] Yucai Lin,†[ab] Donghui Wang,[a] Jipeng Chen,[a] Ke Yang,[a] Binbin Zheng,[a] Weibin Bai,[ab] Rongkun Jian[ab] and Yanlian Xu *[abd]

Silver nanoparticle-based coatings have been regarded as promising candidates for marine antifouling. However, current toxic fabrication methods also lead to environment risks. Nanoparticle agglomeration, poor compatibility with polymer, and rapid release of Ag^+ result in short-term efficacy. In this study, a facile one-pot synthesis method of silver nanoparticles (AgNPs) encapsulated in polymeric urushiol (PUL) was developed. AgNPs were synthesized *in situ* by natural urushiol, serving as a reductant, dispersant and surfactant. Simultaneously, silver nitrate catalyzed the polymerization of urushiol into PUL. This *in situ* reduction method made AgNPs uniformly distributed in the polymer matrix. The binding between the AgNPs and the PUL resulted in the stable release of Ag^+. Results showed the antibacterial rate of a 0.1% AgNPs coating is 100% in laboratory experiments. This environment-friendly coating showed good microbial inhibition performance with long-term (120 days) marine antifouling efficacy. This study shows the potential of preparing an eco-friendly coating with long-term marine antifouling ability.

Received 9th March 2020
Accepted 26th March 2020

DOI: 10.1039/d0ra02205e

rsc.li/rsc-advances

1. Introduction

Marine biofouling, although a natural phenomenon, has been an increasing serious problem to many maritime industrial sectors around the world.[1] Biofouling increases a ship's roughness, reduces the speed of navigation,[2] increases fuel consumption,[3] accelerates the wear-and-tear of equipment, and promotes metal corrosion.[4] It then results in huge economic losses and security risks. To date, the use of marine antifouling coatings remains the most effective way of inhibiting attachment of marine organisms.[5] Several antifouling approaches (*e.g.*, antifoulant releasing coating, biomimetic antifouling materials, *etc.*) have been developed to combat biofouling.[6,7] Among these approaches, the antifoulant releasing coating is the most popular and widely used technology.[8]

The antifoulant releasing coatings consist of the releasing matrices and the active antifoulants compounds or biocides, efficacy of which is critical to the antifouling effects.[9] A variety of antifoulants such as tributyltin (TBT), cuprous oxide, and quaternary ammonium have been developed and widely used. Self-polishing copolymer-based coatings containing TBT was once the best choice due to its high efficacy, however it was globally banned in 2008 due to its deleterious environmental effects.[7] This was followed by copper-based compounds as alternative antifoulants to TBT.[10] Similarly, it was gradually banned due to their ecological risks.[11] Alternatively, silver nanoparticles (AgNPs) are currently widely used in a variety of applications such as water purification,[12] bio-medicine,[13] and food preservatives. It has been considered as a promising antifoulant due to its broad-spectral applications, long-term antibacterial activity, and relatively lower environmental risks.[14] Several AgNPs-based antifouling coatings have been developed but still have several problems. Firstly, the antifouling effect of AgNPs is correlated with the particle size, such that smaller the AgNPs perform better. However, smaller AgNPs are easier to agglomerate.[15] To avoid the agglomeration of AgNPs, potentially risky dispersants or stabilizers are needed during their synthetic production.[16,17] Generally, most of the existing methods to prepare AgNPs are complex or considered as environmental risks because of the used toxic solvents or additives.[18] Secondly, the synthetic AgNPs have poor compatibility with the polymer resin, which will decrease the uniformity of and thus also influencing its antifouling efficiency.[19] Lastly, the AgNPs-based antifouling coating prepared by two-step method has short-term efficiency because of the rapid consumption of Ag^+.[20] Developing a simple, environmentally

[a]*College of Chemistry and Materials, Fujian Normal University, Fuzhou 350007, P. R. China. E-mail: ylxu@fjnu.edu.cn; Tel: +86 59183464353*

[b]*Fujian Provincial Key Laboratory of Polymer Materials, Fuzhou 350007, P. R. China*

[c]*Fujian Provincial Key Laboratory of Advanced Oriented Chemical Engineering, Fuzhou 350007, P. R. China*

[d]*Fujian Engineering Research Center of New Chinese Lacquer Material, Minjiang University, Fuzhou 350007, P. R. China*

† These two authors contributed equally to this work.

friendly, highly efficient, and long-lasting marine antifouling coating is still a significant challenge.

Urushiol, a natural product from raw lacquer that has a catechol derivative with a linear alkenyl group,[21] which not only has bactericidal and antioxidant properties,[22] but also has excellent corrosion resistance and water resistance. Urushiol can be an excellent choice for coatings used in harsh environments and bio-corrosive protection caused by microbial aggregation.[23] Here, we developed a facile one-pot environment friendly method to fabricate AgNPs as marine antifouling coating. Small size AgNPs encapsulated in polymeric urushiol (PUL) were *in situ* synthesized in polymer resins. Urushiol can be used as the dispersant, reducing agent and stabilizer due to its special molecular structure. The urushiol was polymerized simultaneously during the reduction process, where AgNPs were encapsulated in PUL by the interaction of AgNPs and the phenolic hydroxyl group. The AgNPs were uniformly dispersed in the polymer coatings and the Ag^+ of the coatings were steadily released. The antifouling coatings with AgNPs loading showed excellent performance on preventing the attachment of bacteria and inhibiting the growth of algae. In addition, the composite coatings soaked in field for 120 days to demonstrate that the antifouling coatings have good practical antifouling performance.

2. Experimental section

2.1. Materials

Silver nitrate and acetate (>97%) were purchased from Aladdin (Shanghai, China). Urushiol was extracted from raw lacquer procured from Delong Trading Co., Ltd. (Hubei, China). Chlorinated rubber was obtained from Jiangsu Miki Co., Ltd (Jiangsu, China). *Escherichia coli* (*E. coli*) *and Staphylococcus aureus* (*S. aureus*), *Isochrysis zhanjiangensis* (*I. zhanjiangensis*), *Phaeodactylum tricornutum* (*P. tricornutum*) and *Nitzschia closterium* (*N. closterium*) were provided by College of Life Sciences, Fujian Normal University. Carbon steel plates (340 mm × 150 mm × 3 mm) were obtained from Liaocheng Fuwang Metal Materials Co., Ltd. (Shangdong, China).

2.2. Experimental methods

2.2.1. Preparation of PUL/AgNPs. A total of 20 mg mL^{-1} urushiol solution (10 mL) was added dropwise into 10 mg mL^{-1} silver nitrate solution (20 mL) while being continuously stirred at 30 °C. After 2 h reaction, the product was washed with ethanol five times, centrifuged at 12 000 rpm, and dried in the vacuum oven at 45 °C for 12 h.

2.2.2. Preparation of composite coatings. To prepare the composite antifouling coatings, chlorinated rubber (40 g) was first dissolved in butyl acetate. The silver nitrate solution (20 mg mL^{-1}) and the resin solution were also mixed. Subsequently, the urushiol ethanol solution (10 mg mL^{-1}) was added dropwise into the mixed solution. After simultaneously stirring for 2 h, the nanocomposite solution was poured onto a glass substrate (20 mm × 20 mm) for laboratory experiment. Additionally, rosin and organically modified bentonite were added to the mixed solution for complex microbial fouling in the marine. Then the solution was poured onto a carbon steel plate (340 mm × 150 mm × 3 mm) for field marine experiment. The composition of composite coatings for field marine experiment is shown in Table 1. Coatings with different AgNPs mass fractions (0%, 0.05%, 0.1%, 0.3%) were prepared.

2.3. Measuring methods

2.3.1. Characterization. X-ray diffraction (XRD) measurements were conducted on a X'Pert^3 diffractometer (Malvern Panalytical). The infrared spectra of urushiol and PUL/AgNPs were measured using fourier transform infrared spectroscopy (FTIR, Nicolet 5700). Absorption spectra for AgNPs were obtained using the UV-visible spectrophotometer (UV-vis-2600, Shimadzu Corporation). Scanning electron microscope (SEM, JSM-7500F) with an accelerating voltage of 5 kV was used to characterize cross-section morphologies of the different prepared coatings. The presence of silver element signal was characterized by EDX spectroscopy. Transmission electron microscopy (TEM, JEM-2100) was also used to characterize the morphologies of AgNPs and PUL/AgNPs. SEM (Sigma HD) equipped with an EDX spectroscopy to detect the presence and distribution of AgNPs in the coating. The Ag^+ concentration was determined by inductive coupled plasma emission (ICP, Optima 8000).

2.3.2. Ag^+ release testing. The composite coatings (60 mm × 60 mm) were soaked in deionized water (300 mL) at room temperature. Around 10 mL of the solution was taken using a disposable syringe with filtration membrane daily for 15 days, and from these the Ag^+ concentration was determined using ICP.

2.3.3. Antimicrobial assessment. The antibacterial effects of different mass fractions of AgNPs (0%, 0.05%, 0.1%, 0.3%) coatings on Gram-positive *S. aureus* and Gram-negative *E. coli* were measured. Coatings were casted on pre-treated slides (20 mm × 20 mm). *E. coli* and *S. aureus* were cultured on Lauria Broth (LB) agar medium plates at 37 °C until they reached exponential growth stage. Then, 0.5 mL of bacterial suspension were applied to substrates coated with different mass fractions of AgNPs (0%, 0.05%, 0.1%, 0.3%) and further incubated under static condition at 37 °C for 24 h. The unattached bacteria were washed off with 0.01 mol L^{-1} PBS. The films were dehydrated, dried and bacterial adhesion on the coating was observed with SEM. Bare slides were used as the control group.

The antibacterial rates of coatings with different AgNPs content (0%, 0.05%, 0.1%, 0.3%) on *S. aureus* and *E. coli* were measured. The experimental methods were as follows: coatings with different AgNPs content (0%, 0.05%, 0.1%, 0.3%) were cast on pre-treated slides (50 mm × 50 mm). The bacterial suspension was then added to the sample membrane. Subsequently, the dried plastic wrap was covered with the sample and then placed in a constant temperature and humidity incubator. After 24 h, the bacteria on the sample film and the cover film were repeatedly washed into the beaker with 0.01 mol L^{-1} PBS solution. The obtained bacterial suspension was spread on an agar plate and incubated at 37 °C for 24 h. Finally, the effective

Table 1 The composition of composite coatings

Sample	Chlorinated rubber (g)	Rosin (g)	Urushiol (g)	Silver nitrate (mL)	Organically modified bentonite (g)	AgNPs content (%)
a	40	4.53	0	0	0.50	0
b	40	4.53	0.14	3.96	0.50	0.05
c	40	4.53	0.29	7.93	0.50	0.1
d	40	4.53	0.89	23.81	0.50	0.3

colony count was calculated from 20 to 200 colony forming units (CFU), which was counted according to the standard of GB7892-2016 (China) to calculate the antibacterial rate.

I. zhanjiangensis, *P. tricornutum* and *N. closterium* were selected to assess effects of the antifouling coatings on the growth of these phytoplankton. The algae that had grown or reached the exponential phase was utilized for the experiment. Briefly, the coatings were first immersed in the algal culture suspension for 1 day, 3 days and 7 days, at 12 : 12 hour light–dark cycle. The algal cells in the solution were observed and calculated by metallographic microscope.

2.3.4. Antifouling testing. The antifouling performance of the coatings film were obtained by field marine immersion test in accordance with the standard of GB/T 5370-2007 (China). The carbon steel plates (340 mm × 150 mm × 3 mm) were sanded and the surfaces were cleaned up with ethanol. Coatings with different mass fractions of AgNPs (0%, 0.05%, 0.1%, 0.3%) were painted on the steel plates. The steel plates were then immersed in seawater in the East China Sea (+25°76′N, +119°68′E) for 120 days. The plates soaked in the seawater were carefully removed and slightly washed with seawater. Organisms deposited on steel plates were photographed with a digital camera.

3. Results and discussion

3.1. Preparation of PUL/AgNPs

Urushiol, which accounts to 60–70% of the raw lacquer collected from natural resource-rich *Rhus vernicifera*, is a catechol derivative with a linear alkenyl group.[24]

In general, researches have shown that catechol structures can generate semiquinone radicals under the action of enzymes,[25] air,[26] and some inorganic one-electron oxidants (ferric chloride, silver nitrate, copper sulfate, *etc.*),[27–30] and quinone radicals are oxidatively coupled with polyphenols and then form a biphenyl structure. Due to the catechol structure and the unsaturated C=C structure on the side chain of urushiol, some of the quinone radicals react with methylene adjacent to the unsaturated carbon in the side chain, and some of the quinone groups combined with methylene to form a dimer,[31] thereby forming a PUL structure. The urushiol polymerization process includes an oxidative coupling reaction and a side chain crosslinking reaction.

Here, we used urushiol to synthesize AgNPs *in situ*, as illustrated in Fig. 1. The hydroxyl group of urushiol loses one electron to become semi-radical, and the semi-quinone free radical undergoes disproportionation in the presence of oxygen.[32] The active free radicals in urushiol then reduced Ag^+ in the silver nitrate solution. The Ag^+ bonded to the O-site of the urushiol, which prevented the accumulation of AgNPs and the overgrowth of the silver core. The molecular structure of urushiol makes it possible to be used as reductant, dispersant, and surfactant, which can also be crosslinked. Further, as one catalyst for the cross-linking of urushiol, silver nitrate catalyzed the polymerization of urushiol, facilitating AgNPs to be homogenously distributed on the PUL. Consequently, the PUL/AgNPs provided the possibility for long-lasting antifouling activity of the coating.

The TEM images of the as-synthesized PUL/AgNPs are presented in Fig. 2(a) and (b). The spherical shape of AgNPs was observed to be uniformly deposited on the PUL film, with an average particle size of 12.39 nm (Fig. 2(a) inset). The crystal lattice fringe spacing of 0.23 nm was measured (Fig. 2(d)), revealing the cubic crystal lattice structure with (111) plane of metallic silver.[33] Meanwhile, as shown in Fig. 2(f), a strong surface plasmon resonance was centered at 411 nm, indicating the formation of AgNPs in the solution. The EDX of green synthesized AgNPs presented in Fig. 2(e) confirmed the presence of nanocrystalline elemental silver. In addition, the XRD pattern of AgNPs crystals (Fig. 2(h)) clearly shows that five peaks at the two theta positions of 38.1°, 44.3°, 64.4°, 77.4°, and 81.1° were assigned to diffraction from the (111), (200), (220), (311), and (222) planes of face cubic crystal AgNPs (ICDD pattern, 98 005-0882).[33] The crystal form of AgNPs measured in the XRD image was consistent with the results in Fig. 2(d). These clearly

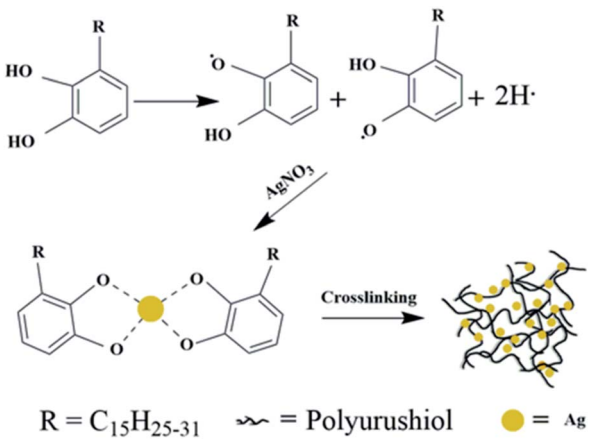

Fig. 1 Schematic *in situ* fabrication of PUL/AgNPs.

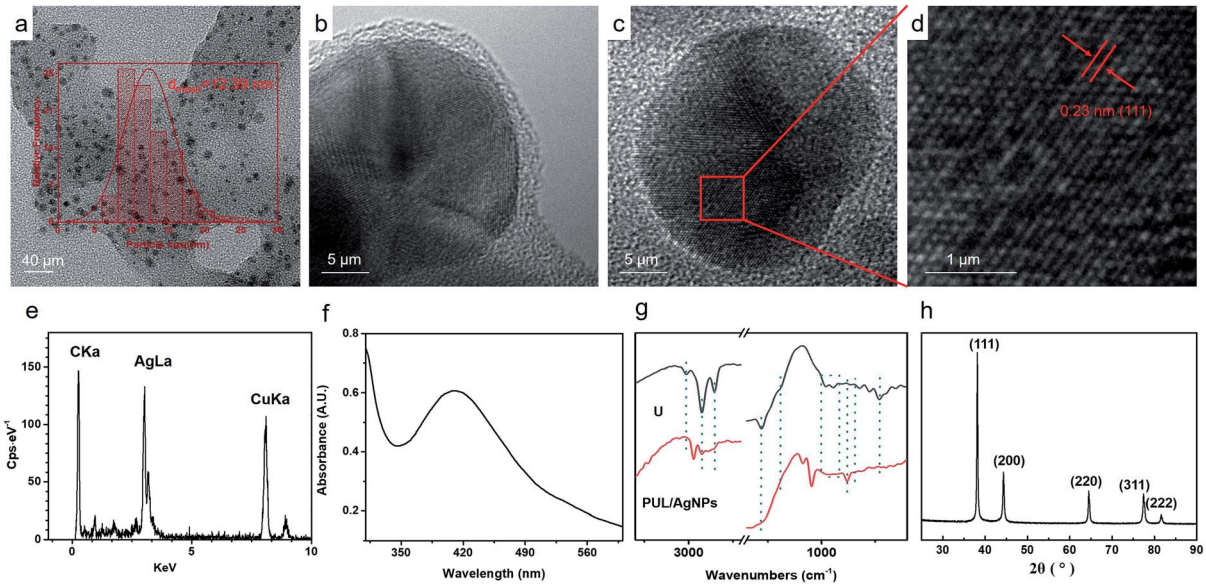

Fig. 2 TEM images of PUL/AgNPs (a–d); EDS of AgNPs (e); UV-vis spectra of AgNPs (f); FT-IR spectra of urushiol (U); PUL/AgNPs (g); XRD image of AgNPs (h).

show that face cubic crystal AgNPs were successfully prepared in this study using urushiol.

Fig. 2(g) shows the FTIR spectrum of the urushiol (U) and PUL/AgNPs. The peak of 2928 cm^{-1} belonging to telescopic vibration of saturated alkyl groups $-CH_2$ was observed. The absorption peak at 2852 cm^{-1} was due to the deformation vibration of $-CH_3$.[34] A peak at 3012 cm^{-1} on the other hand corresponding to the unsaturated group of C–H telescopic vibration in the chain of urushiol disappeared, suggesting that the unsaturated group in the side chain of urushiol were hydrogenated. The peaks at 1280 cm^{-1} and 1189 cm^{-1} were attributed to the bending vibration of –OH. The decrease in the peaks was due to the formation of dimers.[35] Bending vibration absorption peak of hydrogen atoms in benzene ring at 830 cm^{-1} (PUL/AgNPs) was also noted. The increase of the peak at about 870 cm^{-1} and the decrease at 730 cm^{-1} suggest that more substituted groups were formed on the phenyl ring.[36] In contrast, the crab-leg-like peaks 982 cm^{-1} and 945 cm^{-1} belonging to the conjugate alkene groups disappeared in PUL/AgNPs[21] and the appearance of the peak at 969 cm^{-1} (PUL/AgNPs) indicates the formation of *trans*-olefin,[36] potentially associated with the polymerization of urushiol to form PUL during the synthesis of AgNPs.

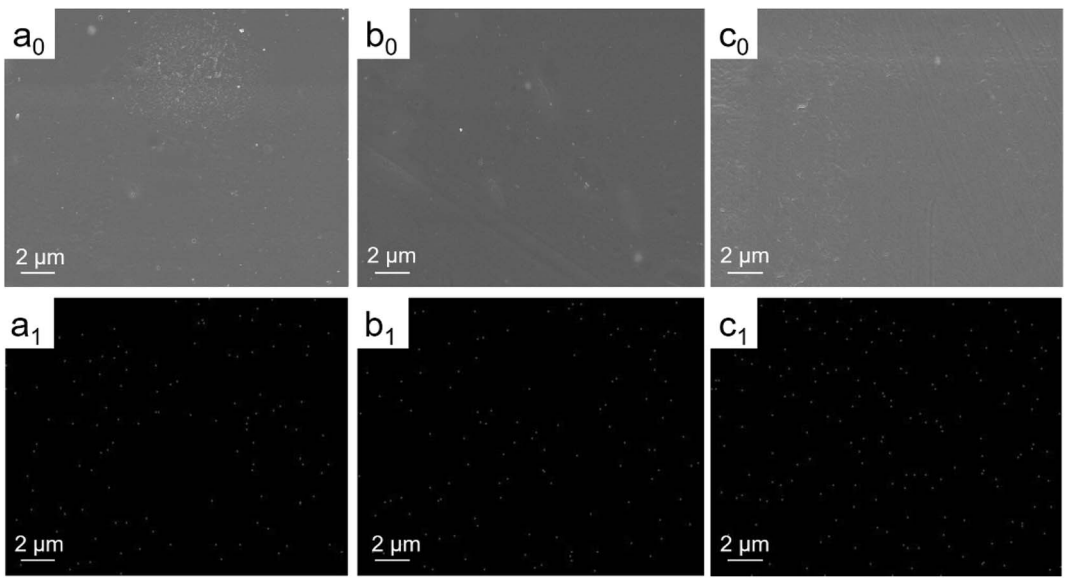

Fig. 3 SEM images (a_0–c_0) and EDS mappings of Ag (a_1–c_1) of 0.05% AgNPs coating (a), 0.1% AgNPs coating (b), 0.3% AgNPs coating (c).

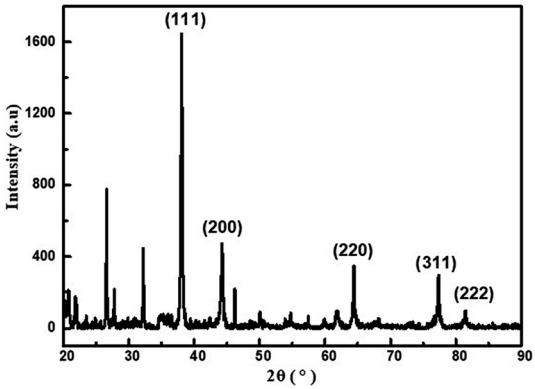

Fig. 4 The XRD pattern of AgNPs in the composite coating.

3.2. Composite coatings characterization and Ag^+ release analysis

Fig. 3(a_0–c_0) indicates that these surfaces of AgNPs coatings were smooth and flat. Fig. 3(a_1–c_1) shows the EDS mappings of silver distribution with different silver content coatings. It shows the presence of silver and the homogeneous distributions of AgNPs in the composite coating.

As shown in Fig. 4, the XRD pattern of AgNPs in the coating clearly shows that five peaks of AgNPs with face cubic crystal structure at the two theta positions, which was consistent with the AgNPs crystal form in PUL/AgNPs. In addition, the average particle diameter of AgNPs in the coating calculated by Debye–Sherrer formula is 17.40 ± 1.40 nm, which was slightly larger than the average particle diameter of AgNPs in PUL/AgNPs (12.39 nm). This may be explained by the slight increase in the particle size of AgNPs due to the presence of other substances during the preparation of the mixed solution.

It can be seen from the Fig. 5(i) that the number of micropores in the coating with PUL/AgNPs. With the relative increase in the content of PUL/AgNPs, the micropores in the coating decrease, which can be explained as AgNPs in the coating had no obvious agglomeration and excellent compatibility of PUL with the resin.

The antimicrobial activity of AgNPs largely depends on the release of Ag^+.[37] Ag^+ release of different coatings is shown in Fig. 5(ii). Further, the Ag^+ release rate was observed to increase with the immersion time, which then exhibited a sustained release afterwards. The release of Ag^+ from the AgNPs coating is related to the degree of erosion of the coating surface.[38] The surface of the coating is slowly eroded by water, and the rate of Ag^+ release decreases. The surface of the coating eroded too quickly, and a large amount of AgNPs were exposed to the aqueous environment,[39] which resulted in the release of Ag^+ burst.

In this study, chlorinated rubber was used as a film-forming substance. It's well known that chlorinated rubber has excellent corrosion resistance and water resistance.[40] During the early stages of coating immersion in the water environment, chlorinated rubber acted as a protective barrier, resulting in a slow Ag^+ release rate in the first stage. The release behaviour at this stage was similar to that reported in the literature.[41] Ag^+ released in the first stage mainly came from AgNPs on or near the surface. With the erosion of chlorinated rubber by water, more AgNPs were more easily exposed to water,[42] the release rate of Ag^+ in the second stage was faster than in the first stage. As the immersing time increases, the release rate of Ag^+ slowed down until a stable release was achieved. One possible reason can be associated with micropores in the coatings as shown in Fig. 5(i). The PUL is considered a "patch" of the coating micropores in the composite coating due to its excellent compatibility with resin. With increased PUL/AgNPs concentration, the micropores in the coating were gradually reduced. The coating became more difficult to be eroded by water, resulting in the Ag^+ release concentration not increasing exponentially with the Ag^+ content in the coatings. The Ag^+ release concentration of 0.05% AgNPs coating was approximately 0.8 μg L^{-1}, while the corresponding values for 0.3% AgNPs coating was 1.2 μg L^{-1}. On the other hand, the urushiol group provided an anchor for the AgNPs, which allowed the AgNPs loaded in the PUL film to be stably released.

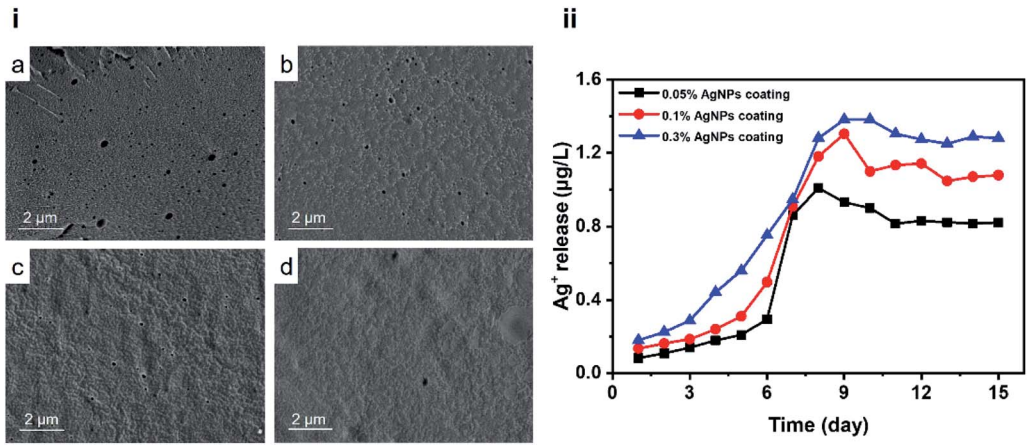

Fig. 5 Cross-section SEM images (i) of the 0% AgNPs coating (a), the 0.05% AgNPs coating (b), the 0.1% AgNPs coating (c) and the 0.3% AgNPs coating (d); Ag^+ release kinetics (ii).

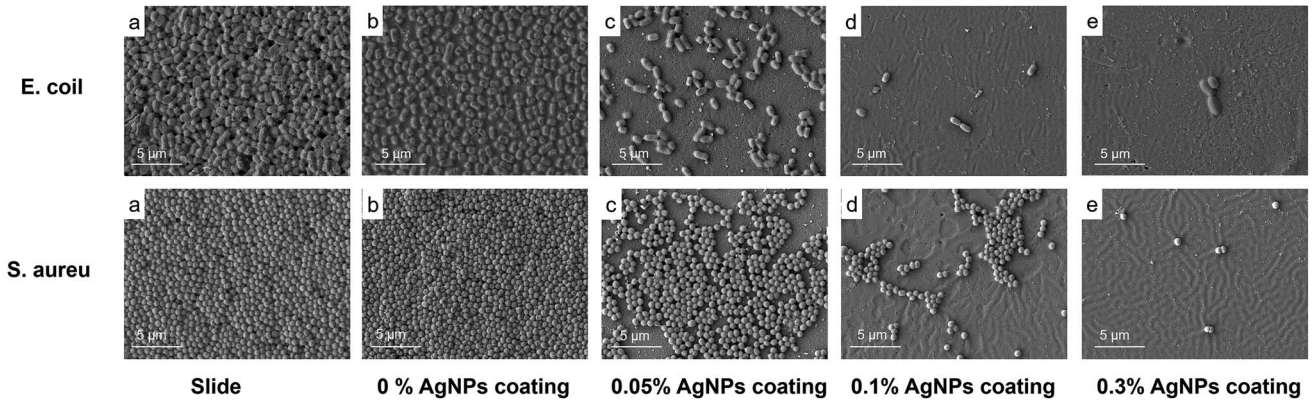

Fig. 6 SEM images of *E. coli* (i) and *S. aureus* (ii) attached to the bare slide (a), the 0% AgNPs coating (b), the 0.05% AgNPs coating (c), the 0.1% AgNPs coating (d), the 0.3% AgNPs coating (e).

Table 2 The antibacterial rate of AgNPs coatings[a]

Antibacterial rate (%)	a	b	c	d	e
S. aureus	0	0	99.43	100	100
E. coli	0	0	99.80	100	100

[a] (a) slide; (b) the 0% AgNPs coating; (c) the 0.05% AgNPs coating; (d) 0.1% AgNPs coating; (e) the 0.3% AgNPs coating.

3.3. Antimicrobial assessments

E. coli and *S. aureus* are the most typical bacteria used to assess the antibacterial activity of antifouling coatings.[43] The SEM images of *E. coli* (i) and *S. aureus* (ii) on the different surfaces (a–e) are shown in Fig. 6. As shown in Fig. 6(a) and (b), the control slide without AgNPs were almost fully colonized by *E. coli* and *S. aureus*, while bacteria abundance that adhered to 0.05% and 0.1% AgNPs coated surfaces had less (Fig. 6(a) and (b)). The 0.3% AgNPs coated surface showed the lowest density of adhered bacteria compared to the other treatments. These results suggest a promising antibacterial efficacy for both *E. coli* and *S. aureus* of AgNPs coatings. In this study, surface with 0.3% AgNPs showed the highest antibacterial potential, with the amount of AgNPs in the coating being much lower than previous studies.[19]

The antibacterial rate of the coatings is shown in Table 2. The antibacterial rate of 0.05% AgNPs against *S. aureus* was 99.43%, and the antibacterial rate against *E. coli* reached 99.80%. When the AgNPs content continues to increase to 0.1%, the antibacterial rate against these two bacteria can reach 100%. It can be seen from the experimental data that with the increase of the content of AgNPs, the antibacterial effect of the coating on *S. aureus* and *E. coli* gradually increased. In addition, when the antibacterial rate has reached 100%, the AgNPs content in the coating was lower than previously reported studies.[44] The excellent antibacterial properties exhibited in the coatings we have developed were actually the result of the synergistic antibacterial effect of AgNPs and urushiol.

We also tested the efficacy of the silver composite against fouling of microalgae including *I. zhanjiangensis*, *P. tricornutum*, and *N. closterium*, which are known to be the most common phytoplankton species in the marine environment. As shown in Fig. 7(a), the amount of *I. zhanjiangensis* cells remained the same in the control even after a day of co-incubation probably due to the low concentration of Ag^+ being released in the solution in the first day, consistent with the results in the Ag^+ release patterns. However, surfaces coated with AgNPs coatings exhibited significant cell inhibition after 3 days, which was also lower than the first day. Notably, a higher amount of AgNPs in the composite coatings resulted in a lower abundance of phytoplankton cells, similar to the results in Fig. 6. After 7 days,

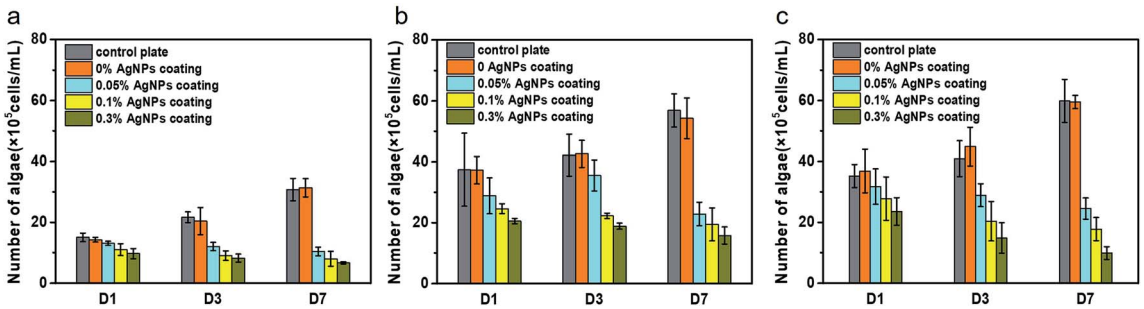

Fig. 7 Cell densities of *I. zhanjiangensis* (a), *P. tricornutum* (b), *N. closterium* (c).

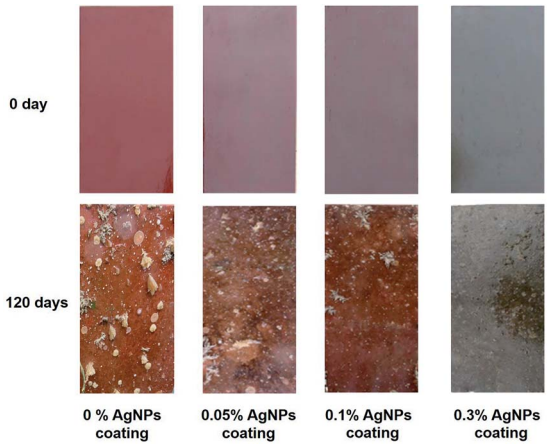

Fig. 8 Images of marine fouling tests of composite coating before and after immersion in sea water for 120 days.

the amount of *I. zhanjiangensis* cells was significantly lower from that of the control plate and 0% AgNPs coating than the third day. For AgNPs coated, it is interesting to note that *I. zhanjiangensis* cells significant decreased with increasing immersion time as shown in Fig. 7(a). This could be explained by the continuous release and accumulation of Ag^+ in the media where the phytoplankton were also suspended. Results showed that Ag^+ was released steadily after 7 days, thus, also resulting in the delayed inhibition of the phytoplankton. Similar results can be drawn from *P. tricornutum* (Fig. 7(b)) and *N. closterium* (Fig. 7(c)). In addition, AgNPs coatings showed stronger inhibition of *P. tricornutum* growth than the other algae.

3.4. Marine field test

To test the long-term applicability of the antifouling performance of AgNPs antifouling coatings in the natural environment, a shallow sea immersion test was conducted. Fig. 8 shows the results of composite antifouling coatings with different AgNPs content. It can be seen that the surface of the plate without AgNPs was considerably fouled by more marine organisms, including algae, barnacles, unidentified larvae and other organisms. Generally, the abundance of barnacle larvae and algae on the surface of the samples were increasing with decreasing concentration of applied AgNPs in the different surfaces. These results were consistent with the experiments on inhibiting microbial growth. In addition, no obvious microbial film was observed on the 0.3% AgNPs coated material, which could be related to Ag^+ activity. An excellent antifouling was observed until after 120 days of incubation underwater in the natural marine environment in surfaces with 0.3% AgNPs.

4. Conclusions

In summary, antifouling composite coatings with different AgNPs content were prepared by *in situ* reduction of urushiol. AgNPs exhibited good dispersion in the coatings. The composite coating was steadily releasing Ag^+, which continued after a certain immersion time, with the concentration of Ag^+ released was related to the PUL/AgNPs content. The antibacterial rate of the coatings against Gram-negative *E. coli* and Gram-positive *S. aureus* increased with increasing AgNPs content. Similar effect was demonstrated in inhibiting the growth of the different microalgae. The composite coatings showed excellent antifouling performance even after 120 days of being submerged under water in a natural marine setting, which could be attributed to the synergistic antifouling effect of AgNPs and PUL. Here, we also showed a method for the synthesis of AgNPs antifouling coating, which was not only not simple but also environmentally friendly, providing a new way of applying AgNPs to marine antifouling coatings.

Conflicts of interest

The authors declare no conflict of interest.

Acknowledgements

This research was supported by National Natural Science Foundation of China (No. 21978050).

References

1 K. Herget, P. Hubach, S. Pusch, P. Deglmann, H. Gotz, T. E. Gorelik, I. A. Gural'skiy, F. Pfitzner, T. Link, S. Schenk, M. Panthofer, V. Ksenofontov, U. Kolb, T. Opatz, R. Andre and W. Tremel, *Adv. Mater.*, 2017, **29**, 1603823.
2 J. Shen, M. Du, Z. Wu, Y. Song and Q. Zheng, *RSC Adv.*, 2019, **9**, 2081–2091.
3 C. S. Ware, T. Smith-Palmer, S. Peppou-Chapman, L. R. J. Scarratt, E. M. Humphries, D. Balzer and C. Neto, *ACS Appl. Mater. Interfaces*, 2018, **10**, 4173–4182.
4 M. S. Selim, M. A. Shenashen, S. A. El-Safty, S. A. Higazy, M. M. Selim, H. Isago and A. Elmarakbi, *Prog. Mater. Sci.*, 2017, **87**, 1–32.
5 Y. Zhang, H. Hu, X. Pei, Y. Liu, Q. Ye and F. Zhou, *Biomater. Sci.*, 2017, **5**, 2493–2500.
6 R. Chen, Y. Li, L. Tang, H. Yang, Z. Lu, J. Wang, L. Liu and K. Takahashi, *RSC Adv.*, 2017, **7**, 40020–40027.
7 K. Feng, C. Ni, L. Yu, W. Zhou and X. Li, *Colloids Surf., B*, 2019, **184**, 110518.
8 A. G. Nurioglu, A. C. C. Esteves and G. de With, *J. Mater. Chem. B.*, 2015, **3**, 6547–6570.
9 I. Banerjee, R. C. Pangule and R. S. Kane, *Adv. Mater.*, 2011, **23**, 690–718.
10 I. Omae, *Chem. Rev.*, 2003, **103**, 3431–3448.
11 Y. Li, Y. Xu, C. C. Fleischer, J. Huang, R. Lin, L. Yang and H. Mao, *J. Mater. Chem. B*, 2018, **6**, 9–24.
12 K. Seetho, S. Zhang, K. A. Pollack, J. Zou, J. E. Raymond, E. Martinez and K. L. Wooley, *ACS Macro Lett.*, 2015, **4**, 505–510.
13 I. A. Wani, S. Khatoon, A. Ganguly, J. Ahmed, T. Ahmad and N. Manzoor, *Colloids Surf., B*, 2013, **101**, 243–250.
14 S. W. P. Wijnhoven, W. J. G. M. Peijnenburg, C. A. Herberts, W. I. Hagens, A. G. Oomen, E. H. W. Heugens, B. Roszek, J. Bisschops, I. Gosens, D. Van De Meent, S. Dekkers,

W. H. De Jong, M. van Zijverden, A. J. A. M. Sips and R. E. Geertsma, *Nanotoxicology*, 2009, **3**, 109–138.
15 G. Benelli, *Parasitol. Res.*, 2016, **115**, 23–34.
16 S. Tang and J. Zheng, *Adv. Healthc. Mater.*, 2018, **7**, 1701503.
17 C. Marambio-Jones and E. M. V. Hoek, *J. Nanopart. Res.*, 2010, **12**, 1531–1551.
18 P.-M. Hannula, S. Pletincx, D. Janas, K. Yliniemi, A. Hubin and M. Lundström, *Surf. Coat. Technol.*, 2019, **374**, 305–316.
19 M. Zhai, Y. Gong, X. Chen, T. Xiao, G. Zhang, L. Xu and H. Li, *Surf. Coat. Technol.*, 2017, **328**, 115–120.
20 M. Rycenga, C. M. Cobley, J. Zeng, W. Li, C. H. Moran, Q. Zhang, D. Qin and Y. Xia, *Chem. Rev.*, 2011, **111**, 3669–3712.
21 J. Yang, F. Shen, J. Deng, J. Cai, Q. Zhang and W. Liu, *J. Appl. Polym. Sci.*, 2018, **135**, 45865.
22 H. S. Kim, J. H. Yeum, S. W. Choi, J. Y. Lee and I. W. Cheong, *Prog. Org. Coat.*, 2009, **65**, 341–347.
23 N. Lone, I. W. Cheong, M. Cho, Y.-K. Hong, Y. S. Choi, S. Perumal, B.-T. Oh and J. Joo, *J. Coat. Technol. Res.*, 2017, **14**, 621–630.
24 I. H. A. M. Arachchilage, M. K. Patel and J. P. Harmon, *Polym. Eng. Sci.*, 2019, **59**, 1611–1623.
25 F. Bruyneel, O. Payen, A. Rescigno, B. Tinant and J. Marchand-Brynaert, *Chemistry*, 2009, **15**, 8283–8295.
26 L. S. Villata, A. M. Berkovic, M. C. Gonzalez and D. O. Martire, *Redox Rep*, 2013, **18**, 205–209.
27 P. Capdevielle and M. Maumy, *Tetrahedron*, 2001, **57**, 379–384.
28 X. Jin, R. Yang, Y. Shang, F. Dai, Y. Qian, L. Cheng, B. Zhou and Z. Liu, *Chin. Sci. Bull.*, 2010, **55**, 2885–2890.
29 R. Ahmed, M. Lehrer and R. Stevenson, *Tetrahedron*, 1973, **29**, 3753–3759.
30 R. S. Mulliken, *J. Am. Chem. Soc.*, 1952, **74**, 811–824.
31 R. Petrucci, P. Astolfi, L. Greci, O. Firuzi, L. Saso and G. Marrosu, *Electrochim. Acta*, 2007, **52**, 2461–2470.
32 D. Wang, M. Zhang, Z. Luo, W. Bai, Y. Xu and J. Lin, *Polym. Bull.*, 2015, **73**, 1639–1647.
33 J. Li, Z. Li, W. Huang, L. Chen, F. Lv, M. Zou, F. Qian, Z. Huang, J. Lu and Y. Li, *Small*, 2019, **15**, 1900436.
34 D. Kim, S. L. Jeon and J. Seo, *Prog. Org. Coat.*, 2013, **76**, 1465–1470.
35 J. Xia, J. Lin, Y. Xu and Q. Chen, *ACS Appl. Mater. Interfaces*, 2011, **3**, 482–489.
36 R. J. Gao, L. W. Wang and Q. Lin, *Prog. Org. Coat.*, 2019, **133**, 169–173.
37 F. J. Osonga, V. M. Kariuki, I. Yazgan, A. Jimenez, D. Luther, J. Schulte and O. A. Sadik, *Sci. Total Environ.*, 2016, **563–564**, 977–986.
38 R. Ma, C. Levard, S. M. Marinakos, Y. Cheng, J. Liu, F. M. Michel, G. E. Brown and G. V. Lowry, *Environ. Sci. Technol.*, 2012, **46**, 752–759.
39 J. Xiong, M. Z. Ghori, B. Henkel, T. Strunskus, U. Schürmann, M. Deng, L. Kienle and F. Faupel, *Appl. Phys. A*, 2017, **123**, 470.
40 S. M. M. Morsi, H. S. Emira, S. M. El-Sawy, R. M. Mohsen and L. A. Khorshed, *Polym. Compos.*, 2018, **40**, 2777–2789.
41 T. Liu, B. Yin, T. He, N. Guo, L. Dong and Y. Yin, *ACS Appl. Mater. Interfaces*, 2012, **4**, 4683–4690.
42 S.-j. Yu, Y.-g. Yin, J.-b. Chao, M.-h. Shen and J.-f. Liu, *Environ. Sci. Technol.*, 2014, **48**, 403–411.
43 A. R. Shahverdi, A. Fakhimi, H. R. Shahverdi and S. Minaian, *Nanomedicine*, 2007, **3**, 168–171.
44 Z. Yang, Y. Wu, J. Wang, B. Cao and C. Y. Tang, *Environ. Sci. Technol.*, 2016, **50**, 9543–9550.